Methods for colloid transport visualization in pore networks

Naoyuki Ochiai,[1] Erika L. Kraft,[2] and John S. Selker[2]

[1] Prediction of colloid transport in the subsurface is relevant to researchers in a variety of fields such as contaminant transport, wastewater treatment, and bioremediation. Investigations have traditionally relied on column studies whereby mechanistic inferences must be drawn on the basis of colloid behavior at the outlet. Over the past decade, development of noninvasive visualization techniques based on visible light, magnetic resonance, and X rays have provided insight into a number of colloid transport mechanisms by enabling direct observation of individual colloids at the pore scale and colloid concentrations at longer length scales. As research focus shifts from transport of ideal colloids in ideal media such as glass beads to natural colloids in natural porous media, these noninvasive techniques will become increasingly useful for studying the collection of mechanisms at work in heterogeneous pore systems. It is useful at this juncture to review recent progress in colloid transport visualization as a starting point for further development of visualization tools to support investigation of colloids in natural systems. We briefly discuss characteristics of visualization systems currently used to study colloid transport in porous media and review representative microscale and mesoscale visualization studies conducted over the past decade, with additional attention given to two optical visualization systems being developed by the authors.

1. Introduction

[2] Colloids are generally defined as particles less than 1 μm in diameter which do not readily settle in water due to their size and density, and are composed of a variety of materials including mineral or rock fragments, mineral precipitates and organic macromolecules, as well as microorganisms (e.g., protozoa, fungi, bacteria, viruses). Colloids may be transported through porous media while suspended in water and are subject to interaction with gas, liquid and solid interfaces. The need to understand the dynamics of colloid transport through the subsurface and other porous media is shared by researchers in a wide range of fields such contaminant transport, wastewater treatment, and bioremediation. For example, colloids may facilitate transport of sediment partitioning contaminants by serving as carriers, thereby accelerating arrival times of these contaminants relative to predictions based on classic solute transport models [*McCarthy and Zachara*, 1989; *Puls and Powell*, 1992; *Corapcioglu and Jiang*, 1993; *Saiers and Hornberger*, 1996; *Kersting et al.*, 1999; *Saiers*, 2002; *de Jonge et al.*, 2004a, 2004b]. Transport of microorganisms in the subsurface is also of interest, both from the standpoint of mitigating pathogen contamination of the subsurface or groundwater, as well as for delivery of microbial agents for bioremediation [*Harvey et al.*, 1989].

[3] In the past thirty years, a significant amount of research has been conducted on colloidal transport through saturated, "ideal" media, such as glass beads or sand, which has yielded a fundamental understanding of the nature of the interaction between colloids and media and the influence of solution chemistry [*McCarthy and McKay*, 2004]. There is a growing awareness, however, that theoretical models based on this understanding have limited applicability to transport in natural systems, which are far more complex than the experimental systems used [*Harvey et al.*, 1993; *Saiers et al.*, 1994; *McCarthy and McKay*, 2004]. Natural media exhibit various types of heterogeneity which can be grouped by the scale at which they occur. Examples of microscale heterogeneities include the surface chemistry and roughness of media grains, as well as surface area and configuration of interfaces. Examples of heterogeneity at the mesoscale include nonrandom distribution of grain and pore shapes and sizes, variations in pore water chemistry, the presence of preferential flow paths or macropores, variability in degree of saturation, and transients in infiltration. In addition, naturally occurring colloids vary significantly in size, shape, density, and surface properties, which influence transport behavior. These heterogeneities may have interacting, nonlinear influence on colloid movement through a medium (e.g., saturation of certain electrostatic binding locations), resulting in complicated perturbations of colloid flux at the outlet.

[4] Most colloid transport experiments have employed media-packed columns to generate "breakthrough" curves, where change in output concentration is measured over time and compared to the source concentration [e.g., *Toran and Palumbo*, 1992; *Harvey et al.*, 1993; *Saiers et al.*, 1994; *Wan and Tokunaga*, 1997; *Schafer et al.*, 1998; *Cumbie and McKay*, 1999; *Silliman et al.*, 2001; *Bradford et al.*, 2002;

---

[1]Department of Crop and Soil Science, Oregon State University, Corvallis, Oregon, USA.
[2]Department of Biological and Ecological Engineering, Oregon State University, Corvallis, Oregon, USA.

Table 1. Fundamental Features of Visualization Techniques

	Resolution Limit	Contrast	Microscale Processes	Mesoscale Processes	Exposure Time	Three-Dimensional	Sample Size	Sources
Visible light imaging	20 μm	fluorescence	no	yes	minutes	no	cm to m	Kraft and Selker [2005], Zhang and Wang [2006] see Tables 2 and 3
Visible light imaging (microscopy)	0.2 μm	fluorescence dark field phase contrast DIC[a]	yes	no	microseconds	no	mm to cm	
Magnetic resonance imaging	10 μm	paramagnetic marker	no	yes	minutes	yes	cm	Sherwood et al. [2003], Seymour et al. [2004]
Synchrotron X-ray tomography	3 μm	dopins	yes	yes	minutes	yes	cm	DiCarlo et al. [2006], Li et al. [2006]
γ-ray tomography	mm	dopins	no	yes	?	yes	cm	Hsieh et al. [1998]
Positron emission tomography	?	radioactive tracer	no	yes	minutes	yes	cm	Khalili et al. [1998]

[a]Differential interference contrast.

Saiers, 2002; *Saiers et al.*, 2003; *Keller et al.*, 2004; *Lenhart and Saiers*, 2004]. This methodology is nonideal for the study of transport in heterogeneous media where multiple mechanisms may have different or even opposite effects on colloid behavior, making interpretation of breakthrough curves difficult. Column dissection following flow-through experiments allows investigators to examine colloid deposition patterns, which may be used to make some mechanistic interpretations of colloid-media interaction [e.g., *Tufenkji et al.*, 2003]. However, destructive sampling does not preserve information about colloid location relative to media grains or various interfaces, which is essential for understanding pore-scale processes, and does not allow observation of processes over time. Given these limitations of column experiments, it is recognized that noninvasive visualization methods can greatly enhance investigation of colloid transport in more heterogeneous and representative media [*Blume et al.*, 2002; *DeNovio et al.*, 2004].

[5] It is conceptually useful to distinguish visualization methods at two scales. Pore-scale/microscale visualization enables researchers to study interaction of individual colloids with air, water, and solid interfaces as influenced by microscale heterogeneities, such as pore configuration and surface roughness or chemistry. Darcy/mesoscale visualization methods, which provide a means to probe the spatial variability of colloid concentrations within a given volume of media, enable investigators to study the effects of pore-scale mechanisms, as well as higher-order media features and heterogeneities, on retention and transport of a population of colloids as they pass through the medium. At both spatial scales, noninvasive visualization can facilitate assessment of the relative importance of different mechanisms, investigation of changes in transport as a function of time or changing conditions, and can lead to discovery of previously unrecognized mechanisms, as illustrated by the visualization of colloid retention at air-water interfaces by *Wan and Wilson* [1994].

[6] Here we review a variety of visualization methods being used to investigate colloid transport in pore networks at both microscale and mesoscale. The paper is organized in four sections, beginning with a discussion of the main characteristics of different visualization methods, followed by reviews of both pore-scale and mesoscale visualization systems which have been used to study colloid transport in porous media, and concluding with a few remarks regarding future developments and promising technologies.

2. Comparisons of Visible Light, Magnetic Resonance, and X-Ray Visualization

[7] Visualization of colloids or fluids in porous media can be achieved by a variety methods based on light, magnetic resonance imaging (MRI), X-ray, γ-ray, or positron emission. Discussion here is limited to methods currently being used or having potential for use in the near future to study colloid transport in porous media. Speculations about promising methods which have not yet been applied to the study of colloids are made at the conclusion of this review. For any study, the appropriate choice of method will depend on the required resolution, sensitivity, dimensional and temporal scale, as well as the nature of the colloids and media used. Qualitative and quantitative imaging parameters for each reported method are provided in Table 1, with the
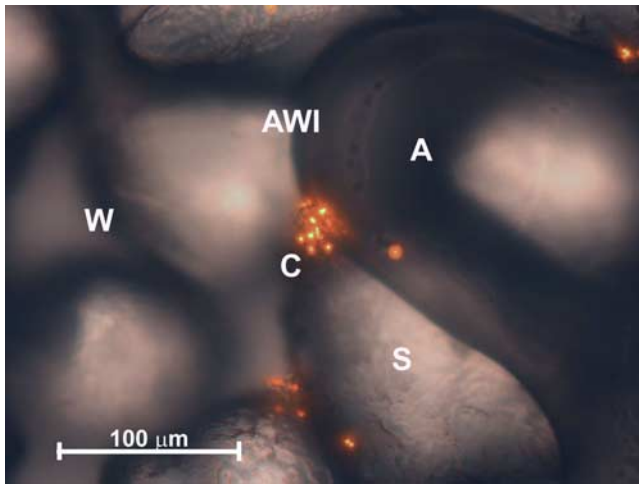
Figure 1. Plan view at 43× magnification of rectangular capillary flow cell developed by *Ochiai et al.* [2005] showing fluorescent 1 μm colloids in relationship to sand grains and air-water interface. W, water phase; A, air phase; AWI, air-water interface; S, sand grains; C, colloids.

caveat that the values reported may change with future technological advances.

[8] The resolution of a given system, defined as the shortest distance between two objects (or two volumes for mesoscale systems) that can be distinguished as separate entities by the observer or camera system, is a function of the type of probe (light, X ray, or radio frequency) and the efficiencies of the imaging system components. Resolution determines the scale of the processes that can be studied and is a critical consideration in experiment design and method selection. It is worth noting that finer-resolution visualization systems generally require use of correspondingly small samples, limiting the scale of media features that can be studied. For light microscopy, resolution is limited by the wavelength of light viewed and the numerical aperture of the optical train of the microscope. Maximum resolution at 10× and 100× magnification using optimized objectives is on the order of 0.60 and 0.20 μm, respectively. For MRI, a maximum resolution of under 4 μm has been reported for imaging a single row of fluorescent polymer beads in a quartz microcapillary [*Ciobanu et al.*, 2002], while resolution of biofilms or colloids in media-packed columns have ranged from 30 μm [*Manz et al.*, 2003] to 200 μm [*Baumann and Werth*, 2005]. For synchrotron-based X-ray imaging, theoretical maximum resolution is several-fold finer than visible light techniques due to the shorter wavelengths of energy utilized. In porous media, maximum resolution of 1 μm may be possible [*Wildenschild et al.*, 2002], however values reported in the literature range from 7.5 μm [*Auzerais et al.*, 1996] to 30 μm [*Li et al.*, 2006]. While all visualization methods mentioned have sufficient resolution for mesoscale investigations, currently, only visible light microscopy methods provide adequate resolution to image individual colloids. Future improvements in MRI or X-ray resolution may make these technologies applicable to pore-scale studies.

[9] A prerequisite for visualization studies is the ability to distinguish colloids from the porous medium and other components of the experimental system, which generally

requires some compromise in choice of colloids and media. Visible light studies commonly utilize fluorescent (or colored) artificial colloids in translucent media such as glass beads or sand (Figure 1) and a frequency selection technique such as the use of band-pass filters to exclude wavelengths of light not associated with the colloid signal in order to increase the signal-to-noise ratio. Artificial colloids, however, are limited approximations of natural colloids, given the wide range in composition, shape, density, and physicochemical surface properties of particles occurring in the field. If natural colloids are to be visualized, some treatment or preparation is usually required to create contrast with the medium. Although several light microscopy techniques are available for enhancing contrast without colloid manipulation (bright field, dark field, differential interference contrast, phase contrast, variable relief contrast, or polarization contrast), these methods may be unable to provide sufficient distinction between colloids and media. Furthermore, these techniques are not applicable to nonmicroscopic visualization. Nonluminescent biological colloids are commonly prepared for visualization by fluorescent staining of specific cell components [e.g., *Li et al.*, 2004] or by development of genetic transformants which express bioluminescent genes such as green fluorescent protein [e.g., *Pesnyakevich and Lyon*, 1998] or lux [e.g., *White et al.*, 1996; *Yarwood et al.*, 2002]. MRI studies require use of paramagnetic colloids or colloids labeled with a paramagnetic material, such as magnetite, to make them "visible" to the system. Figure 2 illustrates the labeling of bacteria with magnetite nanoparticles in preparation for MRI. For X-ray studies, colloids will need to be labeled with a dopin, such as gold [*Li et al.*, 2006] or cadmium [*DiCarlo et al.*, 2006], which is able to attenuate the appropriate X-ray frequency. It is uncertain what impact labeling techniques have on colloid properties, particularly surface chemistry. *Chen and Koopman* [1997] demonstrated significantly altered transport behavior of bacteria that were labeled with some, but not other, nucleic acid fluoro-
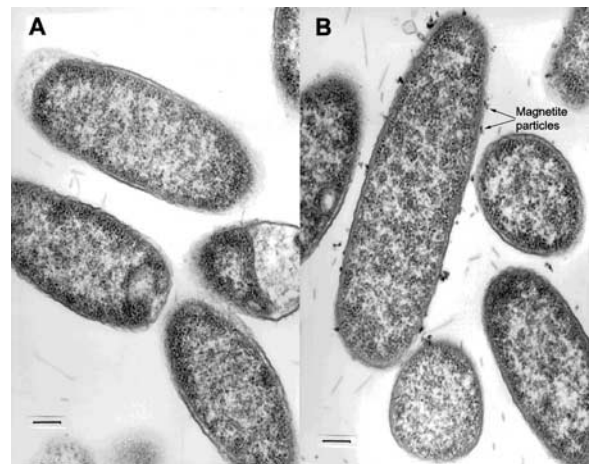

Figure 2. Transmission electron microscopy (TEM) micrographs of *E. coli* K12 NR50 which are (a) unlabeled and (b) labeled with 40 nm diameter magnetite particles. Scale bars represent 200 nm. Reprinted with permission from *Sherwood et al.* [2003]. Copyright 2003 American Chemical Society.

CCD camera

3-way valve

flow-cell or micromodel

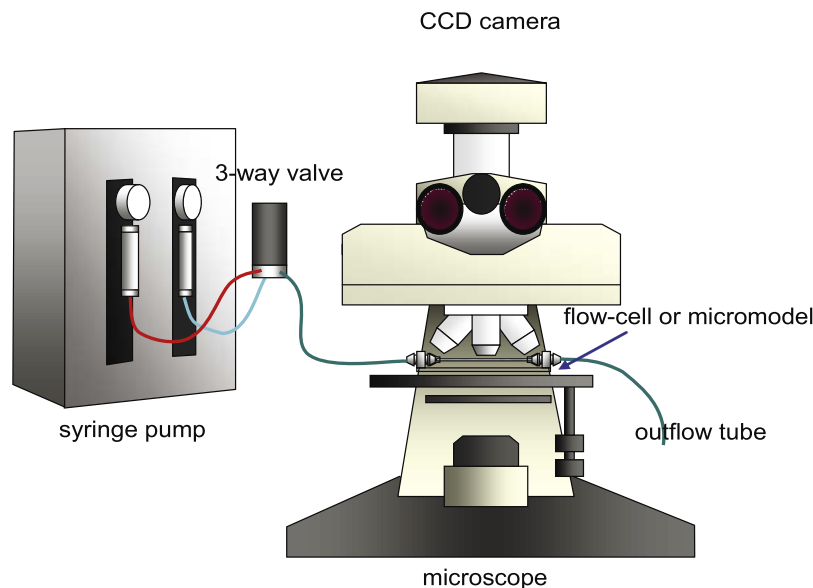syringe pump

outflow tube

microscope

Figure 3. Typical setup of a pore-scale visualization system showing (1) flow cell on microscope stage, (2) imaging system consisting of microscope with CCD camera, and (3) pump to generate fluid flow.

chromes. *Sherwood et al.* [2003] reported no change in motility of bacteria which were labeled with magnetite nanoparticles. In the case of *Phytophthora spp.* (water-molds), labeling of motile zoospores with a fluorophore-conjugated lectin has been shown to cause early encystment and substantial changes in surface chemistry [*Hardham and Suzaki*, 1986]. Thus care must be taken to select labeling materials that have minimal effect on colloid properties relevant to their transport dynamics.

[10] Visualization of colloids in natural media poses several challenges that are difficult to overcome. In visible light systems, colloids can be imaged through translucent media that is several grain layers thick which allows for even packing and reduction of edge effects, but this comes at the cost of signal degradation due to increased attenuation and scattering of both excitation and emitted light. Natural aquifer material is generally opaque, preventing excitation light from reaching colloids and emitted light from reaching the detector. Therefore visible light studies with natural media are limited to thin sections consisting of only one or two grain layers. Even if fluorescence techniques are used, autofluorescence of media grains is likely to interfere with differentiation of colloids from the medium [*Li et al.*, 2004]. While MRI is not affected by media opacity or autofluor-escence, its use to image natural materials may be limited due to signal interference by paramagnetic and ferromag-netic components of the media, such as iron oxides or other metals, as well as organic matter and exchangeable cations [*Hall et al.*, 1997].

[11] Detection limit and sensitivity are important con-straints of visualization systems which measure colloid concentrations. The detection limit refers to the lowest concentration of colloids that can be identified as being present and is typically reported as parts per million mass colloids per mass liquid (ppm), or in particles per unit volume (e.g., particles mL^{-1}). Sensitivity is defined as the smallest change in concentration that can be detected as different. Deposition of colloids in porous media has been demonstrated to be concentration-dependent [*Bradford and Bettahar*, 2006], at least in certain concentration ranges. Ideally, a visualization system should have a low enough detection limit to allow use of colloid concentrations that are observed in nature (10^5–10^{14} particles mL^{-1} [*Kim*, 1991]), and that minimize concentration-dependent artifacts.

[12] The ability to visualize changes in time is very informative of some transport processes, while other pro-cesses may require observation only at discrete time points. The temporal resolution of a given visualization system, defined as the smallest time interval required between distinct visualizations, is dependent on the exposure time necessary to capture images with sufficient contrast and resolution. Currently, light-based microscopy provides the greatest temporal resolution, on the order of milliseconds, and can be used to visualize processes such as advective transport of individual colloids through a pore. Light-based visualization at the mesoscale requires longer exposure, on the order of minutes, depending on the intensity of fluores-cence. Exposure times of MRI and X-ray visualization sys-tems are also on the order of tens of seconds to minutes, and thus would be appropriate for studies that require only single images or sequential images of time-averaged transport.

3. Pore-Scale Visualization Systems

[13] Pore-scale visualization systems generally consist of three main components: (1) a flow cell, (2) a pump to induce fluid motion within the flow cell, and (3) an imaging system (Figure 3). The imaging system usually comprises a conventional or epifluorescent microscope (or magnifying lens) coupled to a video or still image capture device. Flow cells are generally placed horizontally on the existing microscope stage and flow is generated by a syringe or peristaltic pump at either the influent or effluent end of the flow cell. A typical experiment entails pumping a colloid suspension through the flow cell and observing colloids as they transit through the pore network or as they interact with various interfaces (water-solid, air-water, air-water-solid). The following paragraphs describe methods of flow cell

Table 2. Selected Applications of Micromodels for Visualization of Colloidal Transport in Porous Media

Source	Type of Micromodel	Network Characteristics	Pore Dimensions, μm	Visualization Method	Moisture Conditions	Nature of Colloids (Size, μm)	Objective
Wan and Wilson [1994]	etched glass	regular polygon pillars and irregular shapes	200[a]/50[b]; 300[a]/20–100[b]; 4–400	dark-field; epifluorescence	unsaturated	hydrophilic microspheres (0.6, 1.05); hydrophobic microsphere (0.95); bacteria (1.2 × 0.8, 1.0 × 0.8); clay (0.5)	attachment at the air-water interface
Wan et al. [1996]	etched glass	two-domain: fracture-matrix	range of widths 0–600[c]	epifluorescence	saturated	microspheres (1.0)	two-domain flow
Lanning and Ford [2002]	etched glass	regular cylindrical pillars	360–375 × 60–83[c]	light scattering to determine turbidity	saturated	*E. coli*	dispersion of bacteria
Sirivithayapakorn and Keller [2003a]	etched silicon	simulation of natural pore system	2.4 – 30 × 15[c]	epifluorescence	saturated	latex microspheres (0.05, 1.0, 2.0, 3.0); stained bacteriophage	size exclusion and colloid acceleration
Sirivithayapakorn and Keller [2003b]	etched silicon	simulation of natural pore system	2.4 – 30 × 15[c]	epifluorescence	unsaturated	latex microspheres (0.05, 1.0, 2.0, 3.0); stained bacteriophage	dissolution of air-water interface
Auset and Keller [2004]	molded silicon (PDMS[d])	rounded square pillars	10, 20 × 12[c]	epifluorescence	saturated	latex microspheres (2,3,5,7)	colloid dispersion
Baumann and Werth [2004]	etched silicon	regular cylindrical pillars	173[a]/35[b] × 50[c]	epifluorescence	saturated	microspheres (0.691,1.96)	comparison to LB model and filtration theory predictions[e]
Auset et al. [2005]	molded silicon (PDMS[d])	simulation of natural pore system	2.4 – 30 × 12[c]	epifluorescence	cyclical infiltration and draining	DAPI stained bacteria (2 × 1); latex microspheres (5)	Intermittent filtration of bacteria and colloids
Chen and Flury [2005]	etched glass	regular cylindrical pillars	70	bright field	unsaturated	natural colloids(0.348), modified colloids (0.368), kaolinite (0.332), Na-montmorillonite (0.324)	retention of mineral colloid in unsaturated media

[a]Diameter or range of diameters for pore body, when specified in the paper.
[b]Diameter or range of diameters for pore throat, when specified in the paper.
[c]Depth or range of depths of pore system, when specified in paper.
[d]Polydimethylsiloxane.
[e]LB, lattice Boltzman.

Table 3. Applications of Media-Packed Flow Cells for Visualization of Colloidal Transport Through Porous Media

Source	Dimensions (L × W × D), cm	Grain Size, μm	Type of Microscopy	Moisture Conditions	Nature of Colloids (Size, μm)
Crist et al. [2004]	26.0 × 4.8 × 0.5	430–600	CCD camera attached to video microscopic lens	unsaturated	nonfluorescent blue colloids (0.3,0.8)
Crist et al. [2005]	26.0 × 4.8 × 0.5	850–1700	CCD camera attached to video microscopic lens	unsaturated	nonfluorescent blue colloids (4.8,5.2)
Bradford et al. [2005, 2006]	7.0 × 2.0 × 0.2	150; 710/150	Epi-fluorescence	saturated	latex microspheres (1.1, 3.0)
Zevi et al. [2005]	22.0 × 2.0 × 0.5	850–1700	bright field	unsaturated	hydrophilic latex microspheres (0.8,2.6,4.8); hydrophobic latex microsphere (5.2)
Ochiai et al. [2005]	5.0 × 0.1 × 0.01	50–100	bright field and epifluorescence	saturated, unsaturated	fluorescently stained cysts (8–10), latex microspheres (1.0)
Gao et al. [2006]	6.0 × 1.6 × 0.3	355–425	bright field and epifluorescence	unsaturated, infiltration and draining	latex microspheres (2.0) GFP-transformed *E. coli*

fabrication and summarize investigations which have used pore-scale visualization.

[14] Two types of flow-through systems are currently being employed to visualize movement of individual colloids at the pore scale: micromodels and media-packed flow cells. Characteristics of these systems are summarized in Tables 2 and 3. Glass micromodels are constructed by etching a pore network pattern and its mirror image onto two glass plates which are fused face to face at high temperatures [*Wan and Wilson*, 1994]. Silicon micromodels have been constructed by photochemically etching a pore network pattern onto a silicon wafer and anodically bonding a glass plate to the top of the wafer and an aluminum [*Baumann and Werth*, 2004] or a glass [*Keller et al.*, 1997] plate to the bottom for support. Molded silicone micromodels have been fabricated by pouring poly(dimethylsiloxane) (PDMS) into a mold consisting of an etched silicon wafer, followed by curing and polymerization with a slab of precured PDMS to form a closed channel system [*Auset and Keller*, 2004]. Pore network patterns are transferred to glass or silicon plates by first coating the plates with ultraviolet (UV) light sensitive photoresist, placing a lithography mask (with a negative pattern) over the plate, and then exposing areas which are to be etched to UV light. Computer controlled lithography enables both precise control of the network geometry and accurate replication between plates (Figure 4). Micromodel pore networks are two-dimensional in a topological pore network sense, though some three-dimensional features are expressed at the pore scale, including pore wedge features that exist where plates meet [*Wan and Wilson*, 1994]. Additionally, pores of different depths on the same plate can be achieved by sequential etching [*Wan et al.*, 1996]. The surface chemistry of micromodels depends on the composition of the material used, and is generally considered to be homogeneous. The glass used by *Wan and Wilson* [1994] consisted of 72% SiO_2, 14% Na_2O, 3.8% CaO, and other trace metal oxides, while the main components of silicon wafers used by *Sirivithayapakorn and Keller* [2003a] were silica and silicon hydroxides. When water wet, the surface was covered with surface hydroxyl groups and negatively charged at neutral pH. The PDMS is hydrophobic and has an air-water contact angle of approximately 109° [*Auset and Keller*, 2004], but can be rendered hydrophilic by sodium silicate treatment [*Auset et al.*, 2005].

[15] The utility of visualization techniques in the study of colloid transport is illustrated by the initial micromodel application by *Wan and Wilson* [1994], which revealed the role of air-water interfaces as potential sites for colloid retention. Subsequent investigations using micromodels (summarized in Table 2) have led to a variety of advances including verification of putative mechanisms such as size exclusion [*Sirivithayapakorn and Keller*, 2003a] or film straining [*Gao et al.*, 2006], and evaluation of predictive models based on fluid dynamics and transport theory [*Auset and Keller*, 2004; *Baumann and Werth*, 2004]. Glass micromodels introduced by *Wan et al.* [1996] and etched silicon micromodels developed by *Rangel-German and Kovscek* [2006] contain both fracture and matrix fields and are potential tools for studying two-domain flow. Employing glass micromodels with spatially periodic pore networks, *Lanning and Ford* [2002] studied bacterial dispersion during saturated transport and chemotaxis under stagnant fluid conditions. Using silicon micromodels with realistic pore geometries (Figure 4a), Sirivithayapakorn and Keller visualized both accelerated transport of colloids relative to the bulk liquid due to size exclusion and the presence of preferential pathways [*Sirivithayapakorn and Keller*, 2003a], and the fate of latex microspheres and bacteriophages during dissolution of trapped air bubbles [*Sirivithayapakorn and Keller*, 2003b]. *Baumann and Werth* [2004] visualized transport of 0.7 and 2.0 μm fluorescent colloids through silicon micromodels with a regular pore pattern (Figure 4b) to evaluate the accuracy of flow path and particle velocity predictions based on a 2-D lattice Boltzmann (LB) model and filtration efficiency predictions based on colloid filtration theory. *Auset and Keller* [2004] studied particle trajectories, residence times, and dispersion coefficients for
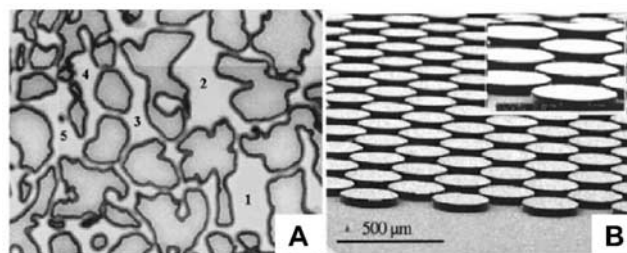

Figure 4. Examples of micromodels with (a) pore pattern copied from thin slice of a porous media [from *Sirivithayapakorn and Keller*, 2003b] and (b) regular pore network (reprinted from *Baumann and Werth* [2005], copyright 2005, with permission from Elsevier).
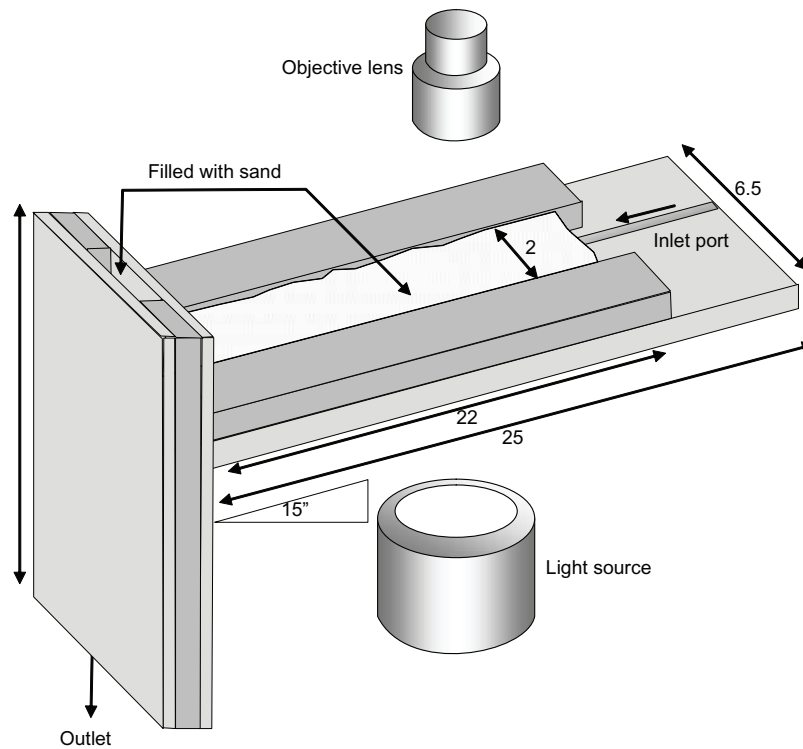
Figure 5. Schematic of tilted, open-faced visualization chamber utilized by *Crist et al.* [2004, 2005] and *Zevi et al.* [2005], showing chamber dimensions and positioning of video magnification lens and light source. Adapted with permission from *Zevi et al.* [2005] Copyright 2005 American Chemical Society.

different sized colloids in idealized pore networks of PDMS micromodels. *Auset et al.* [2005] employed PDMS models with irregular pore geometry to investigate intermittent transport of bacteria and latex microspheres during cyclical infiltration and draining events. Using variably saturated glass micromodels, *Chen and Flury* [2005] observed the lack of attachment of naturally occurring and wastewater-treated colloids, pure kaolinite, or Na-montmorillonite to the liquid-gas interface.

[16] Flow cells packed with granular media are also being used to visualize colloids at the pore scale (summarized in Table 3). *Crist et al.* [2004, 2005] developed an open-faced infiltration chamber filled with quartz sand (850 to 1700 μm) to a depth of 0.5 cm (Figure 5). A unique feature of this flow chamber is that it is mounted at an angle between 15° and 45°. This system was used to investigate retention of hydrophilic and hydrophobic colloids at the air-water-solid (AWS) and water-solid (WS) interfaces in unsaturated media [*Crist et al.*, 2004, 2005; *Zevi et al.*, 2005] as well as to image water flow through water films using confocal microscopy [*Zevi et al.*, 2005]. The possibility that the open chamber face results in artifacts of evaporation remains a point of contention [*Steenhuis et al.*, 2005; *Wan and Tokunaga*, 2005]. *Gao et al.* [2006] constructed flow cells from transparent acrylic, which were fitted with stainless steel membranes at the inlet and outlet ends to maintain capillary pressure, and packed with quartz sand (grain size range 355 to 425 μm) to a porosity of 0.4 (Figure 6). Using this flow cell, they observed mobilization and retention dynamics of 2.0 μm fluorescently dyed latex microspheres in various compartments of partially saturated sand under various moisture contents and flow regimes. *Bradford et al.*

[2005] designed a 0.2 × 2.0 × 7.0 cm flow cell (150 and 710 μm) to visualize straining of 1.1 and 3.0 μm sulfate colloids at textural interfaces in homogeneous (150 μm) or layered (750/150 μm) sand, and to investigate the role of straining in microbial deposition [*Bradford et al.*, 2006].

[17] A flow cell system under development by our group [*Ochiai et al.*, 2005] (Figure 7) consists of a rectangular glass capillary (#5010, Vitrocom, Mountain Lakes, NJ) packed with a monolayer of media grains. Capillaries are available in various dimensions (depths from 20 to
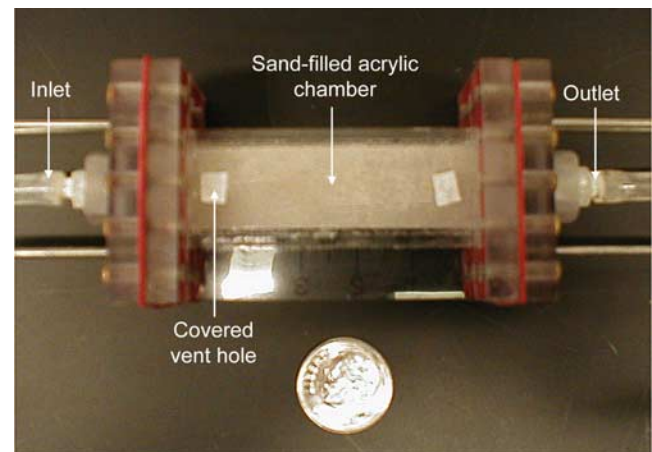

Figure 6. Quartz-sand packed visualization flow cell constructed from acrylic plates used in the work of *Gao et al.* [2006].
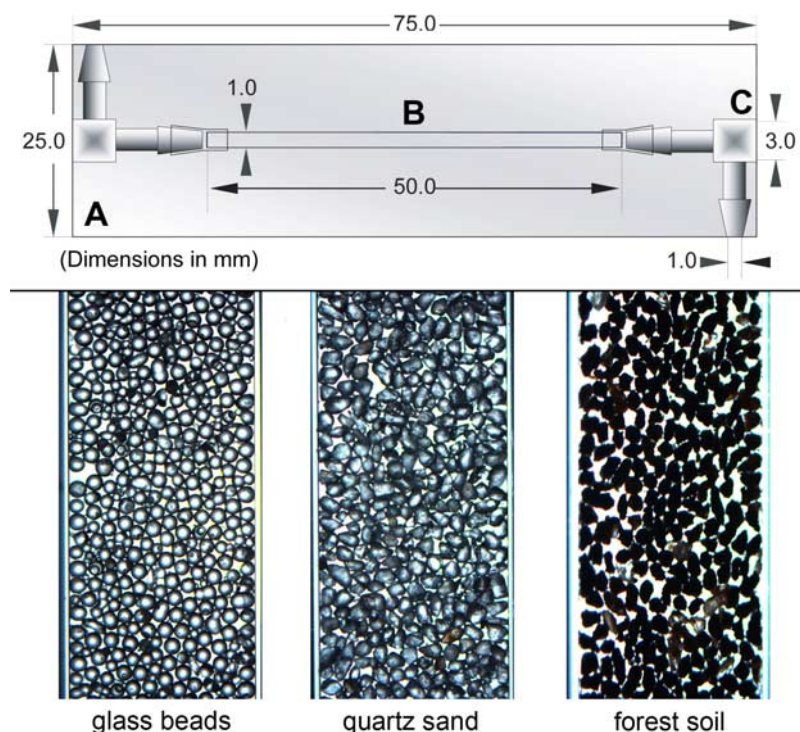
Figure 7. (top) Schematic of media-packed flow-cell under development by *Ochiai et al.* [2005], showing rectangular glass capillary with internal dimensions 0.1 × 1.0 mm (A) connected to 1.6 mm barbed nylon elbows (B) and mounted on a standard glass slide (C). (bottom) Examples of capillaries packed with 90 μm diameter glass beads, quartz sand, and forest soil.

1000 μm). A nylon mesh with 35 μm openings is attached on either end of the capillary to prevent loss of media. Capillaries are connected to other components of the flow system via microbore tubing and 1.6 mm (0.0625 in) barbed nylon connectors which also serve to mount the capillaries to a microscope slide. The rectangular profile of the capillary provides two transparent flat faces through which media grains and colloids can be viewed without distortion associated with wall curvature. Rectangular capillaries of various depths (20 to 1000 μm) are available and can be adapted for flow cell use. We are using 0.1 × 1.0 × 50 mm capillaries with a 0.1 mm wall that approximates the thickness of a standard microscope slide cover slip (0.17 mm), allowing use of high-magnification objectives with standard working distances. These capillary flow cells are currently being used to investigate transport of *Phytophthora* spp. zoospores and cysts in saturated and unsaturated media.

[18] Edge effects created by the flow cell walls are a concern for current pore-scale visualization systems. Thus materials should be chosen with careful consideration of colloid characteristics to minimize system artifacts associated with the visualization system itself. The current systems are predominantly horizontally oriented and effects of gravity are assumed to be unimportant over the spatial and temporal scale of experiments. This assumption, however, may not be valid for larger or denser colloids, whose settling behavior may have an impact on transport. These potential shortcomings aside, the benefits gained from direct observation of microscale processes warrant continued use of these visualization systems. The ability to design and fabricate precise pore geometries and relative homogeneity

of pore surfaces makes micromodels particularly useful for investigations that focus on pore geometry and interfaces. At the same time, since the etched models are fundamentally two-dimensional networks rather than three-dimensional granular structures, many critical aspects of pore-scale geometry may not be well represented in comparison to field conditions (e.g., isolated pores, pendant water, dendritic flow paths, and heterogeneous surface composition). The use of media-packed flow cells enables the visualization of colloid behavior in more realistic 3D pore spaces, and thus colloid interaction with more natural air-water interfacial configurations. These types of systems are therefore well suited to the study of pore-scale colloid behavior under partially or variably saturated media. In addition, the potential to use any type of media grain in flow cells introduces the possibility of investigating effects of media heterogeneity (physical or chemical) on interactions of colloids, media, and air-related interfaces. To date, however, investigations using media-packed flow cells have been conducted using quartz sands with well-established characteristics. The utility of micromodels for studying chemical or physical (roughness) surface heterogeneity remains to be explored and depends on the development of methods to manipulate surface properties with fairly high spatial resolution as demonstrated by *Auset and Keller* [2006].

4. Mesoscale Visualization Systems

[19] While pore-scale visualization methods enable investigation of mechanisms affecting individual or small populations of colloids, they have limited applicability at greater length scales where larger-scale media features play
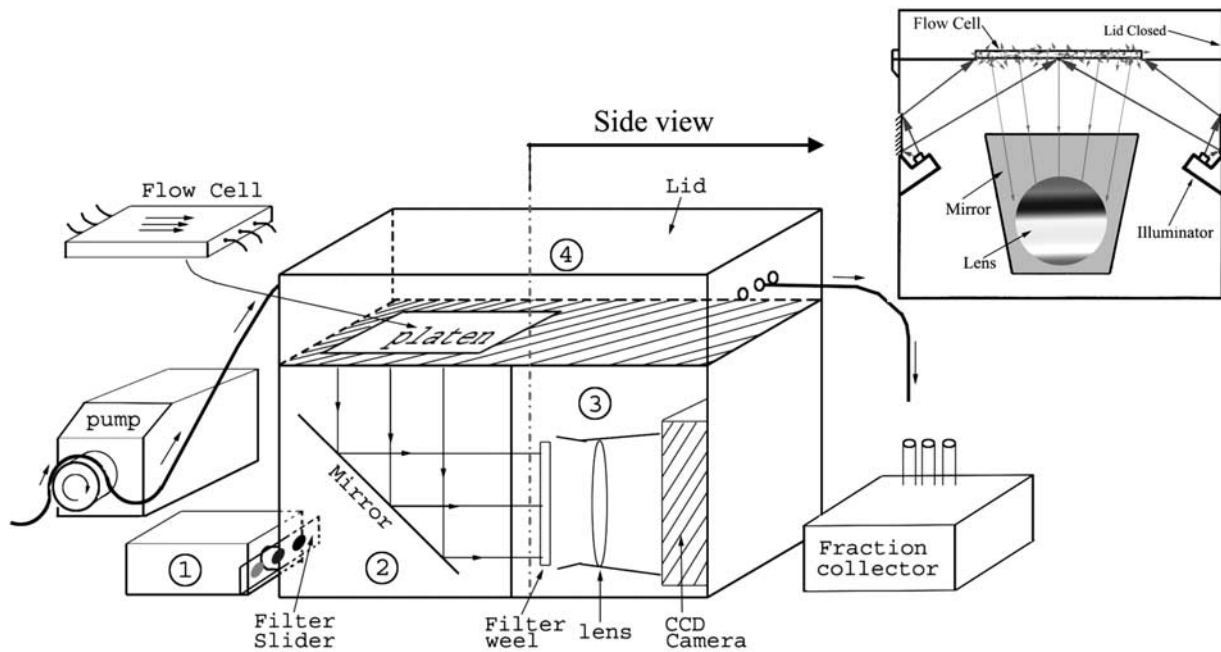
Figure 8. Schematic of mesoscale epifluorescence imaging system developed by *Zhang and Wang* [2006] showing illuminator (1), closed optical path image (COPI) chamber (2), capture system chamber (3), and sample chamber (4).

a major role [*Sun et al.*, 2001]. At the mesoscale (here defined as 10–1000 times the pore scale) heterogeneities such as nonrandom distribution of grain and pores shapes and sizes, textural inclusions, variability in saturation, gradients in pore water chemistry, local pore clogging, or presence/evolution of preferential flow paths are expected to affect overall colloid movement through and retention within a medium. Mesoscale visualization methods do not track individual colloids but enable observation of colloid concentrations in a given volume of media. In addition to providing a means to validate upscaling of pore-scale mechanisms to behavior of colloid populations at the column length scale, mesoscale visualization can aid in investigation of the influence of various media heterogeneities and features on colloids populations as they pass through the medium.

[20] The basic setup of mesoscale visualization systems is analogous to that of pore-scale systems, and entails (1) a media-packed flow cell, (2) a means to generate fluid flow, and (3) an imaging system. Physical dimensions and configuration of flow cells vary widely from system to system and are critical considerations as they determine the length scale of media features that can be investigated. Imaging in mesoscale systems is also constrained by parameters such as detection limit, sensitivity, and spatial or temporal resolution which may determine their applicability to a given study. Briefly, the three types of visualization systems currently under development discussed here are (1) epifluorescent systems developed by *Zhang and Wang* [2006] and *Bridge et al.* [2006], (2) a transmitted fluorescence system employed by *Kraft and Selker* [2005], and (3) MRI systems utilized by *Sherwood et al.* [2003], *Olson et al.* [2004], and *Baumann and Werth* [2005].

[21] A light-based mesoscale visualization method developed by *Zhang and Wang* [2006] utilizes a horizontally oriented $20 \times 20 \times 1$ cm flow cell packed with quartz sand, mounted within a light-tight box (Figure 8). Excitation light from a 150 Watt halogen lamp is filtered and directed into a closed optical path image chamber and through an optical-grade transmittable acrylic viewing window where fluorescent latex particles in the flow cell are excited. Emitted light is reflected off a $45°$ angle mirror, passed through an emission filter and collected by a 14-bit, cooled charge-coupled device (CCD) camera that resides in a separated chamber of the light-tight box. Each pixel in the resultant 1024×1024 pixel array can be resolved to an area as small as $400 \ \mu m^2$. Placement of the source and detector on the same side of the flow cell is intended to reduce the amount of excitation light that enters the detector and the sensitivity of the system is reported at $\sim 2 \times 10^5$ particles mL^{-1} (approximately 0.1 ppm). The system has been used to observe nonexponentially decreasing deposition of colloids as a function of pore water velocity near a radial injection point. A second reflexive (epifluorescent) mesoscale imaging system has been developed [*Bridge et al.*, 2006] which utilizes UV light to illuminate fluorescent colloids and conservative tracer as they are coadvected through a vertically oriented $200 \times 100 \times 6.7$ mm chamber packed with quartz sand. Pixel resolution of this system is $0.478 \ mm^2$, and pixel data have a dynamic range of 256 brightness values. This system has been used to calculate attachment efficiencies with varying ionic strength.

[22] The experimental system being developed by our group [*Kraft and Selker*, 2005; *Weisbrod et al.*, 2003b] consists of parallel glass plates (45×60 cm) held vertically in an air-tight manifold to form a 1 cm thick inner chamber which is filled with granular media (Figure 9). Colloid suspensions or other fluids are introduced into the chamber by multiple inlets located at the top of the sand pack, and effluent is collected at drainage points at the bottom of the
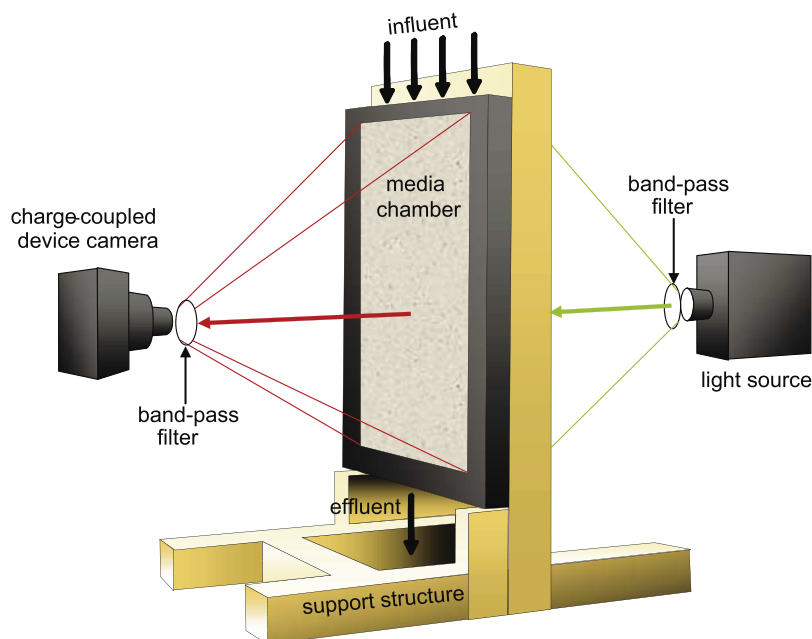
Figure 9. Schematic of mesoscale light transmission visualization under development by *Kraft and Selker* [2005], showing arrangement of optical components and media chamber. Note: not drawn to scale.

chamber. Fluorescent colloids in the porous media are excited by an incandescent 100 Watt lamp on one side of the chamber and light emitted from colloids is detected by a CCD camera located on the side opposite the light source. The detection limit has been improved 100-fold [*Kraft and Selker*, 2005] by placing narrow band-pass filters in front of both the light source (filter 32054, Chroma Corp, Trenton, NJ) and the CCD (filter 41293), to exclude light off-frequency from peak excitation or emission wavelengths. The system employs a 512×512 pixel scientific-grade CCD camera (Princeton Instruments, Roper Scientific, Trenton, NJ) with exceptionally large photodiodes (29×29 μm) to allow detection of low light intensities (10 photons per pixel) over 260,000 individual points, with a 16-bit linear dynamic range. The resulting system detection limit, given a particle diameter of 1 μm and density of 1.055 g/cm^3, is on the order of 0.6 ppm (Figure 10), or approximately 9×10^5 particles mL^{-1}. Further improvements in detection limit are expected through installation of a light source with higher output in the target spectral band (e.g., LEDs). Spatial resolution of this system is on the order of 1 mm. Spatial resolution can be increased using a different camera, but since light is averaged across the 1 cm thickness of the chamber, spatial resolution less than 1 mm provides no additional information. Captured images are pseudocolorized to accentuate differences in emitted light intensity, which are then correlated to colloid concentrations. Time-lapse image capture enables investigation of mass transport of colloids through the experimental plane over time.

[23] The porous media visualization system described above has been used to investigate a wide range of variably saturated transport processes. These investigations include the observation and/or quantification of the following: fingered flow [*Selker et al.*, 1992a], wetting front instability [*Selker et al.*, 1992b], water content [*Niemet and Selker*,

2001], imbibition of saline solutions [*Weisbrod et al.*, 2002], air-water interfacial area [*Niemet et al.*, 2002], vapor transport [*Parker et al.*, 2006; *Weisbrod et al.*, 2003a], colloid concentration [*Weisbrod et al.*, 2003b], and microbial growth [*Rockhold et al.*, 2006; *Uesugi et al.*, 2001; *Yarwood et al.*, 2002, 2006]. The *Weisbrod et al.* [2003b] study showed results indicating that colloidal particles will be retained at the capillary fringe (Figure 11). Investigation of
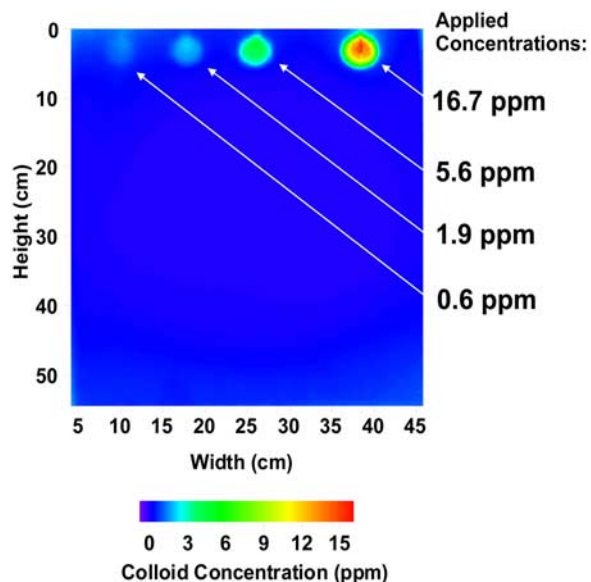

Figure 10. Processed and pseudocolorized light transmission image from the *Kraft and Selker* [2005] system of four colloid plumes of different concentration in 30/40 silica sand. The detection of the 0.6 ppm ($\sim$9 $\times$ 10^5 particles mL^{-1}) plume represents a hundredfold improvement on the system's detection limit as a result of improved signal-to-noise ratio.
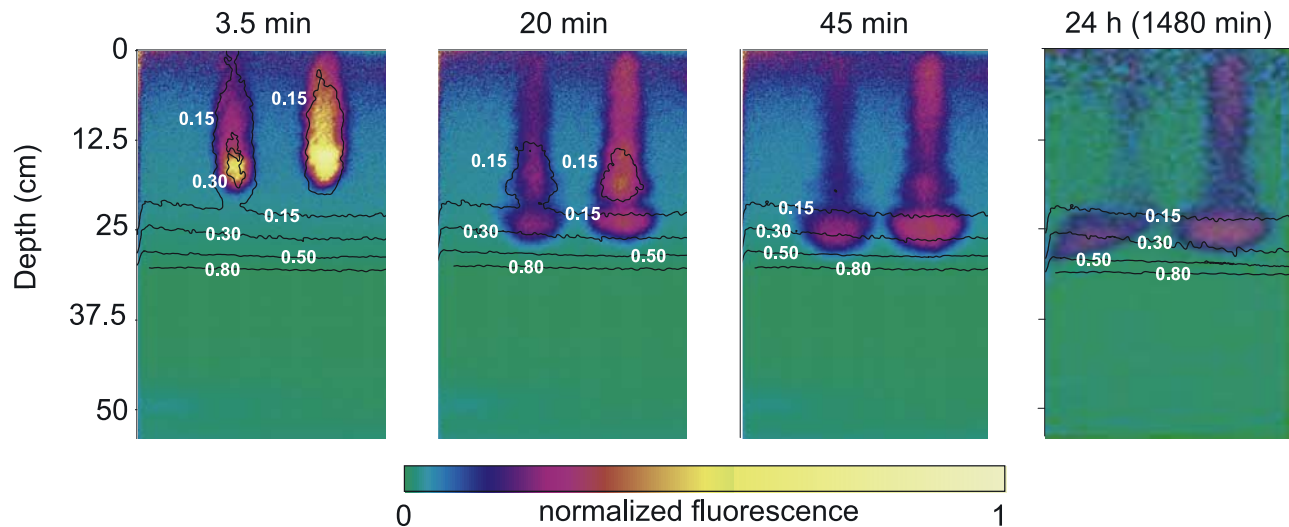
Figure 11. Processed time series of colloid fluorescence light transmission images over 1480 min. Plumes are 0.04% concentration of 0.02 μm (left) and 1.0 μm (right) latex microspheres encountering the capillary fringe, where the black lines are water content contours. Reprinted with permission from *Weisbrod et al.* [2003b]. Copyright 2003 American Chemical Society.

microbial growth in the chamber has resulted in a model of microbial density as a function of light emission that can predict biomass over four orders of magnitude, and observation has been made of colony growth against the direction of flow [*Yarwood et al.*, 2002].

[24] Visualization systems based on MRI have been developed by several groups [*Potter et al.*, 1996; *Sherwood et al.*, 2003; *Baumann and Werth*, 2005]. Flow cells consist of cylindrical columns ranging in diameter from 1 to 1.5 cm and in length from 7.5 to 8 cm. Columns have been packed with 250 to 300 μm diameter glass-coated polystyrene microbeads [*Sherwood et al.*, 2003] or with silica gel ranging in size from 250 to 1000 μm [*Baumann and Werth*, 2005]. Imaging is accomplished by placing the column within a magnetic resonance spectrometer system, and requires use of paramagnetic colloids or labeling of colloids with paramagnetic materials. *Sherwood et al.* [2003] were able to visualize diffusion in a water-saturated porous medium of motile and nonmotile bacteria labeled with 50–60 nm diameter magnetite particles at a spatial resolution of 330 μm. Utilizing the same visualization setup, Olson et al. investigated chemotactic response of magnetite-labeled *Pseudomonas putida* F1 [*Olson et al.*, 2004] and retarded diffusion of *P. putida* F1 in porous media relative to a conservative solute and *Escherichia coli* NR50 [*Olson et al.*, 2005]. *Baumann and Werth* [2005] observed retarded transport of 1.28 μm diameter superparamagnetic colloids (density 1.726 g cm^{-3}) through 250–600 μm silica gel compared to 850–100 μm silica gel. The maximum voxel resolution achieved by this system was 200 $\times$ 200 $\times$ 1000 μm. An example of images generated by the MRI system developed by *Baumann and Werth* [2005] is presented in Figure 12.

[25] Mesoscale visualization systems span a range of spatial scales. While methods development efforts often focus on improving spatial resolution, these refinements must be weighed against the concomitant reduction in sample size and scale of features that can be studied. In general, resolution should be optimized for the length scale of interest. The MRI systems presented here are limited in size and may be most appropriate for studies of small-scale media heterogeneities such nonrandom distribution of different grain types (size, shape, composition). MRI systems with lower resolution but which allow for larger samples may be suitable for investigation of higher-order media features and heterogeneities. Detection limit and system sensitivity are particularly relevant to the discussion of mesoscale visualization systems which track colloid concentrations. The minimum colloid concentrations detectable by the light-based systems described here (10^5–10^6 particles mL^{-1}) fall in the lower range of naturally occurring concentrations (10^5–10^{14} particles mL^{-1}) reported by *Kim* [1991]. Detection limits of the MRI systems are not as well documented, but for the system developed by *Baumann and Werth* [2005], appear to be on the order of 10^8 particles mL^{-1} (approximately 55 ppm). Colloid deposition for 1 μm particles has been shown to be concentration-dependent at concentrations of 9.7 $\times$ 10^6 to 7.7 $\times$ 10^7 particles mL^{-1} [*Bradford and Bettahar*, 2006] (approximately 5.4 to 42.5 ppm), suggesting that interpretation of results from mesoscale visualization studies should take into account potential concentration dependence. Currently, both visible light and MRI visualization methods have limited utility for imaging colloid transport in natural material due to media opacity and signal interference by media components such as paramagnetic and ferromagnetic particles, clay, or organic matter [*Hall et al.*, 1997]. Development of engineered media, which better approximate features of natural media such as surface roughness and chemistry while retaining characteristics necessary for visualization, may extend the utility of current light and MRI-based visualization systems.

5. Summary and Conclusions

[26] Over the past decade, visualization studies have contributed to the elucidation of several mechanisms rele-
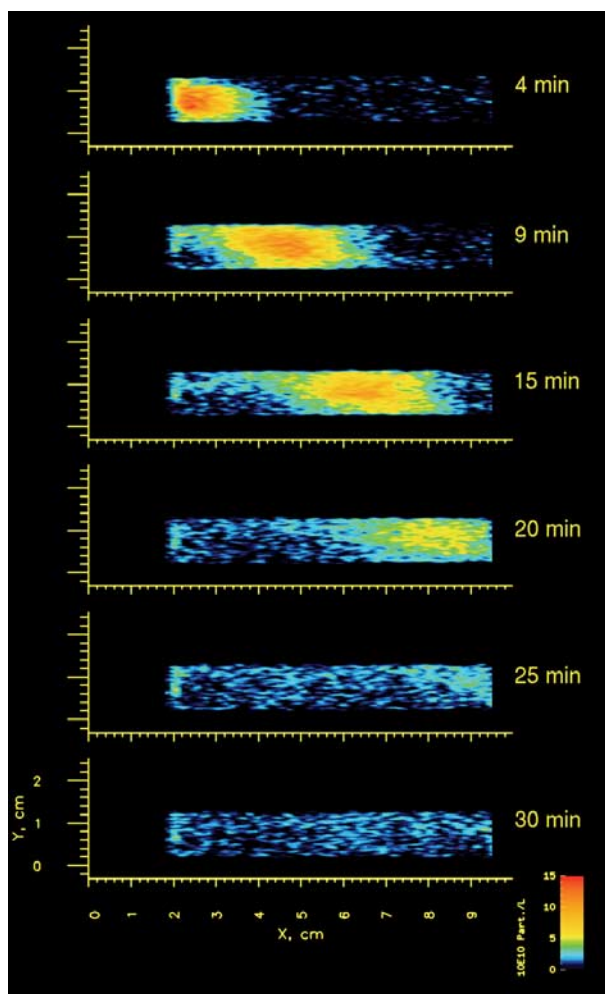
Figure 12. Time series magnetic resonance images illustrating superparamagnetic colloid propagation (left to right) through column packed with silica gel. Axes are column height and length in cm and the color bar indicates colloid concentration in 1×10^{11} particles L^{-1}. Reprinted from *Baumann and Werth* [2005], copyright 2005, with permission from Elsevier.

vant to transport of colloids in the subsurface. While the majority of studies to date have focused on pore-scale processes, light and MRI-based mesoscale systems under development are suitable for investigation of higher-order media features and heterogeneities, while novel methods demonstrate the potential to span both length scales [*Yoon et al.*, 2006]. Notwithstanding these advances, a limitation of current visualization methods is their dependence on "ideal" media such as glass, silica gels, or sand, and artificial colloids, which do not adequately simulate the variability in shape, composition, or surface characteristics of natural colloids or media. Thus a key challenge that remains is the development of tools to investigate transport of natural colloids in natural porous media.

[27] One approach to addressing this challenge is to develop visualization techniques which allow imaging of colloids directly in natural media. The opacity of most natural media precludes use of light-based visualization methods and presence of iron oxide may confound use of MRI. With requisite optimization of detection limits, sensi-

tivity, as well as spatial and temporal resolution, imaging techniques based on X-ray [*Thieme et al.*, 2003; *DiCarlo et al.*, 2006; *Li et al.*, 2006], γ-ray [*Hsieh et al.*, 1998], or positron emission [*Khalili et al.*, 1998] may in the future enable imaging of colloid concentrations or even individual colloids in intact soil cores.

[28] An alternative approach is to engineer colloids and media which have specific "nonideal" physical and chemical characteristics yet retain properties such as translucence which are critical for visualization. This approach, illustrated by column studies utilizing iron oxyhydride-modified sand [*Johnson et al.*, 1996] or aminosilane-modified glass beads [*Ko and Chen*, 2000], can be extended to engineering of media grains with various chemical as well as physical properties, such as shape or roughness [*Yoon et al.*, 2006], which are expected to affect colloid transport [*Saiers and Ryan*, 2005].

[29] With technological improvements of current visualization methods, development of novel noninvasive techniques, and engineering of artificial colloids and media which better approximate those found in natural systems, it is certain that visualization studies will continue to play an important role in advancing understanding of colloid transport in the subsurface.

References

Auset, M., and A. A. Keller (2004), Pore-scale processes that control dispersion of colloids in saturated porous media, *Water Resour. Res.*, 40, W03503, doi:10.1029/2003WR002800.

Auset, M., and A. A. Keller (2006), Pore-scale visualization of colloid straining and filtration in saturated porous media using micromodels, *Water Resour. Res.*, 42, W12S02, doi:10.1029/2003WR004639.

Auset, M., A. A. Keller, F. Brissaud, and V. Lazarova (2005), Intermittent filtration of bacteria and colloids in porous media, *Water Resour. Res.*, 41, W09408, doi:10.1029/2004WR003611.

Auzerais, F., J. Dunsmuir, B. Ferreol, N. Martys, J. Olson, T. Ramakrishnan, D. Rothman, and L. Schwartz (1996), Transport in sandstone: A study based on three dimensional microtomography, *Geophys. Res. Lett.*, 23, 705–708.

Baumann, T., and C. J. Werth (2004), Visualization and modeling of polystyrol colloid transport in a silicon micromodel, *Vadose Zone J.*, 3, 434–443.

Baumann, T., and C. J. Werth (2005), Visualization of colloid transport through heterogeneous porous media using magnetic resonance imaging, *Colloids Surf. A*, 265, 2–10.

Blume, T., N. Weisbrod, and J. S. Selker (2002), Permeability changes in layered sediments: Impact of particle release, *Ground Water*, 40, 466–474.

Bradford, S., and M. Bettahar (2006), Concentration dependent transport of colloids in saturated porous media, *J. Contam. Hydrol.*, 82, 99–117.

Bradford, S. A., S. R. Yates, M. Bettahar, and J. Simunek (2002), Physical factors affecting the transport and fate of colloids in saturated porous media, *Water Resour. Res.*, 38(12), 1327, doi:10.1029/2002WR001340.

Bradford, S. A., J. Simunek, M. Bettahar, Y. F. Tadassa, M. T. van Genuchten, and S. R. Yates (2005), Straining of colloids at textural interfaces, *Water Resour. Res.*, 41, W10404, doi:10.1029/2004WR003675.

Bradford, S. A., J. Simunek, and S. L. Walker (2006), Transport and straining of E. coli O157:H7 in saturated porous media, *Water Resour. Res.*, 42, W12S12, doi:10.1029/2005WR004805.

Bridge, J. W., S. A. Banwart, and A. L. Heathwaite (2006), Noninvasive quantitative measurement of colloid transport in mesoscale porous media using time lapse fluorescence imaging, *Environ. Sci. Technol.*, 40, 5930–5936.

Chen, G., and M. Flury (2005), Retention of mineral colloids in unsaturated porous media as related to their surface properties, *Colloids Surf. A*, 256, 207–216.

Chen, J., and B. Koopman (1997), Effect of fluorochromes on bacterial surface properties and interaction with granular media, *Appl. Environ. Microbiol.*, 63, 3941–3945.

Ciobanu, L., D. Seeber, and C. Pennington (2002), 3D MR microscopy with resolution 3.7 m by 3.3 m by 3.3 m, *J. Magn. Reson.*, 158, 178–182.

Corapcioglu, M. Y., and S. Jiang (1993), Colloid-facilitated groundwater contaminant transport, *Water Resour. Res.*, 29, 2215–2226.

Crist, J. T., J. F. McCarthy, Y. Zevi, P. Baveye, J. A. Throop, and T. S. Steenhuis (2004), Pore-scale visualization of colloid transport and retention in partly saturated porous media, *Vadose Zone J.*, 3, 444–450.

Crist, J. T., Y. Zevi, J. F. McCarthy, J. A. Throop, and T. S. Steenhuis (2005), Transport and retention mechanisms of colloids in partially saturated porous media, *Vadose Zone J.*, 4, 184–195.

Cumbie, D. H., and L. D. McKay (1999), Influence of diameter on particle transport in a fractured shale saprolite, *J. Contam. Hydrol.*, 37, 139–157.

de Jonge, L. W., C. Kjaergaard, and P. Moldrup (2004a), Colloids and colloid-facilitated transport of contaminants in soils: An introduction, *Vadose Zone J.*, 3, 321–325.

de Jonge, L. W., P. Moldrup, G. H. Rubaek, K. Schelde, and J. Djurhuus (2004b), Particle leaching and particle-facilitated transport of phosphorus at field scale, *Vadose Zone J.*, 3, 462–470.

DeNovio, N. M., J. E. Saiers, and J. N. Ryan (2004), Colloid movement in unsaturated porous media: Recent advances and future directions, *Vadose Zone J.*, 3, 338–351.

DiCarlo, D. A., Y. Zevi, A. Dathe, S. Giri, B. Gao, and T. S. Steenhuis (2006), In situ measurements of colloid transport and retention using synchrotron X-ray fluorescence, *Water Resour. Res.*, 42, W12S05, doi:10.1029/2005WR004850.

Gao, B., J. Saiers, and J. Ryan (2006), Pore-scale mechanisms of colloid deposition and mobilization during steady and transient flow through unsaturated granular media, *Water Resour. Res.*, 42, W01410, doi:10.1029/2005WR004233.

Hall, L. D., M. H. G. Amin, E. Dougherty, M. Sanda, J. Votrubova, K. S. Richards, R. J. Chorley, and M. Cislerova (1997), MR properties of water in saturated soils and resulting loss of MRI signal in water content detection at 2 tesla, *Geoderma*, 80, 431–448.

Hardham, A., and E. Suzaki (1986), Encystment of zoospores of the fungus, *Phytophthora cinnamomi*, is induced by specific lectin and monoclonal antibody binding to the cell surface, *Protoplasma*, 133, 165–173.

Harvey, R. W., L. H. George, R. L. Smith, and D. R. LeBlanc (1989), Transport of microspheres and indigenous bacteria through a sandy aquifer: Results of natural- and forced-gradient tracer experiments, *Environ. Sci. Technol.*, 23, 51–56.

Harvey, R. W., N. E. Kinner, D. Macdonald, D. Metge, and A. Bunn (1993), Role of physical heterogeneity on the interpretation of small-scale laboratory and field observations of bacteria, microbial-sized microsphere, and bromide transport through aquifer sediments, *Water Resour. Res.*, 29, 2713–2721.

Hsieh, H., G. Brown, and M. Stone (1998), Measurement of porous media component content and heterogeneity using gamma ray tomography, *Water Resour. Res.*, 34, 365–372.

Johnson, P., N. Sun, and M. Elimelech (1996), Colloid transport in geochemically heterogeneous porous media: Modeling and measurements, *Environ. Sci. Technol.*, 30, 3284–3293.

Keller, A. A., M. J. Blunt, and P. V. Roberts (1997), Micromodel observation of the role of oil layers in three-phase flow, *Transp. Porous Media*, 26, 277–297.

Keller, A. A., S. Sirivithayapakorn, and C. V. Chrysikopoulos (2004), Early breakthrough of colloids and bacteriophage MS2 in a water-saturated sand column, *Water Resour. Res.*, 40, W08304, doi:10.1029/2003WR002676.

Kersting, A. B., D. W. Efurd, D. L. Finnegan, D. J. Rokop, D. K. Smith, and J. L. Thompson (1999), Migration of plutonium in ground water at the Nevada Test Site, *Nature*, 397, 56–59.

Khalili, A., A. Basu, and U. Pietrzyk (1998), Flow visualization in porous media via positron emission tomography, *Phys. Fluids*, 10, 1031–1033.

Kim, J. (1991), Actinide colloid generation in groundwater, *Radiochim. Acta*, 52/53, 71–81.

Ko, C., and J. Chen (2000), Dynamics of silica colloid deposition and release in packed beds of aminosilane-modified glass beads, *Langmuir*, 16, 6906–6912.

Kraft, C. E., and J. S. Selker (2005), Methodological developments in in-situ measurement and visualization of colloid transport processes in the subsurface, paper presented at Geological Society of America Annual Meeting and Exposition, Salt Lake City, Utah.

Lanning, L. M., and R. M. Ford (2002), Glass micromodel study of bacterial dispersion in spatially periodic porous networks, *Biotechnol. Bioeng.*, 78, 556–566.

Lenhart, J. J., and J. E. Saiers (2004), Adsorption of natural organic matter to air-water interfaces during transport through unsaturated porous media, *Environ. Sci. Technol.*, 38, 120–126.

Li, X., C. Lin, J. D. Miller, and W. P. Johnson (2006), Pore-scale observation of microsphere deposition at grain-to-grain contacts over assemblage-scale porous media domains using X-ray microtomography, *Environ. Sci. Technol.*, 40, 3762–3768.

Li, Y., W. A. Dick, and O. H. Tuovinen (2004), Fluorescence microscopy for visualization of soil microorganisms: A review, *Biol. Fertil. Soils*, 39, 301–311.

Manz, B., F. Volke, D. Goll, and H. Horn (2003), Measuring local flow velocities and biofilm structure in biofilm systems with magnetic resonance imaging (MRI), *Biotechnol. Bioeng.*, 84, 424–432.

McCarthy, J. F., and L. D. McKay (2004), Colloid transport in the subsurface: Past, present, and future challenges, *Vadose Zone J.*, 3, 326–337.

McCarthy, J. F., and J. M. Zachara (1989), Subsurface transport of contaminants, *Environ. Sci. Technol.*, 23, 496–502.

Niemet, M. R., and J. S. Selker (2001), A new method for quantification of liquid saturation in 2D translucent porous media systems using light transmission, *Adv. Water Resour.*, 24, 651–666.

Niemet, M. R., M. L. Rockhold, N. Weisbrod, and J. S. Selker (2002), Relationships between gas-liquid interfacial surface area, liquid saturation, and light transmission in variably saturated porous media, *Water Resour. Res.*, 38(8), 1135, doi:10.1029/2001WR000785.

Ochiai, N., M. Dragila, and J. Parke (2005), Use of rectangular capillary chambers for nondestructive microscopic observation of biofilm on sand, *Eos Trans. AGU*, 86(52) Fall Meet. Suppl., Abstract B31A-0963.

Olson, M. S., R. M. Ford, J. A. Smith, and E. J. Fernandev (2004), Quantification of bacterial chemotaxis in porous media using magnetic resonance imaging, *Environ. Sci. Technol.*, 38, 3864–3870.

Olson, M. S., R. M. Ford, J. A. Smith, and E. J. Fernandez (2005), Analysis of column tortuosity for $MnCl_2$ and bacterial diffusion using magnetic resonance imaging, *Environ. Sci. Technol.*, 39, 149–154.

Parker, L., R. Yarwood, and J. Selker (2006), Observations of gas flow in porous media using a light transmission technique, *Water Resour. Res.*, 42, W05501, doi:10.1029/2005WR004080.

Pesnyakevich, A., and G. Lyon (1998), Transformation of *Erwinia carotovora* ssp. atroseptica with the green fluorescent protein gene from Aequorea Victoria, *J. Phytopathology*, 146, 57–60.

Potter, K., R. L. Kleinberg, F. J. Brockman, and E. W. McFarland (1996), Assay for bacteria in porous media by diffusion-weighted NMR, *J. Magn. Reson., Ser. B*, 113, 9–15.

Puls, R. W., and R. M. Powell (1992), Transport of inorganic colloids through natural aquifer material: Implications for contaminant transport, *Environ. Sci. Technol.*, 26, 614–621.

Rangel-German, E. R., and A. R. Kovscek (2006), A micromodel investigation of two-phase matrix-fracture transfer mechanisms, *Water Resour. Res.*, 42, W03401, doi:10.1029/2004WR003918.

Rockhold, M. L., R. R. Yarwood, M. R. Niemet, P. J. Bottomley, F. J. Brockman, and J. S. Selker (2006), Visualization and modeling of the colonization dynamics of a bioluminescent bacterium in variably saturated, translucent quartz sand, *Adv. Water Resour.*, in press.

Saiers, J. E. (2002), Laboratory observations and mathematical modeling of colloid-facilitated contaminant transport in chemically heterogeneous systems, *Water Resour. Res.*, 38(4), 1032, doi:10.1029/2001WR000320.

Saiers, J. E., and G. M. Hornberger (1996), The role of colloidal kaolinite in the transport of cesium through laboratory sand columns, *Water Resour. Res.*, 32, 33–41.

Saiers, J., and J. Ryan (2005), Colloid deposition on non-ideal media: The influences of collector shape and roughness on the single-collector efficiency, *Geophys. Res. Lett.*, 32, L21406, doi:10.1029/2005GL024343.

Saiers, J. E., G. M. Hornberger, and C. Harvey (1994), Colloidal silica transport through structured, heterogeneous porous media, *J. Hydrol.*, 163, 271–288.

Saiers, J. E., G. M. Hornberger, D. B. Gower, and J. S. Herman (2003), The role of moving air-water interfaces in colloid mobilization within the vadose zone, *Geophys. Res. Lett.*, 30(21), 2083, doi:10.1029/2003GL018418.

Schafer, A., P. Ustohal, H. Harms, F. Stauffer, T. Dracos, and A. J. B. Zehnder (1998), Transport of bacteria in unsaturated porous media, *J. Contam. Hydrol.*, 33, 149–169.

Selker, J. S., P. Leclerq, J.-Y. Parlange, and T. Steenhuis (1992a), Fingered flow in two dimensions: 1. Measurement of matric potential, *Water Resour. Res.*, 28, 2513–2521.

Selker, J. S., J. Y. Parlange, and T. Steenhuis (1992b), Wetting front instability in homogeneous sandy soils under continuous infiltration, *Soil Sci. Soc. Am. J.*, 56, 1346–1350.

Seymour, J. D., S. L. Codd, E. L. Gjersing, and P. S. Stewart (2004), Magnetic resonance microscopy of biofilm structure and impact on transport in a capillary bioreactor, *J. Magn. Reson.*, 167, 322–327.

Sherwood, J. L., J. C. Sung, R. M. Ford, E. J. Fernandez, J. E. Maneval, and J. A. Smith (2003), Analysis of bacterial random motility in a porous medium using magnetic resonance imaging and immunomagnetic labeling, *Environ. Sci. Technol.*, 37, 781–785.

Silliman, S. E., R. Dunlap, M. Fletcher, and M. A. Schneegurt (2001), Bacterial transport in heterogeneous porous media: Observations from laboratory experiments, *Water Resour. Res.*, 37, 2699–2707.

Sirivithayapakorn, S., and A. Keller (2003a), Transport of colloids in saturated porous media: A pore-scale observation of the size exclusion effect and colloid acceleration, *Water Resour. Res.*, 39(4), 1109, doi:10.1029/2002WR001583.

Sirivithayapakorn, S., and A. Keller (2003b), Transport of colloids in unsaturated porous media: A pore-scale observation of processes during the dissolution of air-water interface, *Water Resour. Res.*, 39(12), 1346, doi:10.1029/2003WR002487.

Steenhuis, T. S., J. F. McCarthy, J. T. Crist, Y. Zevi, P. C. Baveye, J. A. Throop, R. L. Fehrman, A. Dathe, and B. K. Richards (2005), Reply to "Comments on 'Pore-scale visualization of colloid transport and retention in partly saturated porous media'," *Vadose Zone J.*, 4, 957–958.

Sun, N., M. Elimelech, N. Z. Sun, and J. N. Ryan (2001), A novel two-dimensional model for colloid transport in physically and geochemically heterogeneous porous media, *J. Contam. Hydrol.*, 49, 173–199.

Thieme, J., G. Schneider, and C. Knochel (2003), X-ray tomography of a microhabitat of bacteria and other soil colloids with sub-100 nm resolution, *Micron*, 34, 339–344.

Toran, L., and A. V. Palumbo (1992), Colloid transport through fractured and unfractured laboratory sand columns, *J. Contam. Hydrol.*, 9, 289–303.

Tufenkji, N., J. A. Redman, and M. Elimelech (2003), Interpreting deposition patterns of microbial particles in laboratory-scale column experiments, *Environ. Sci. Technol.*, 37, 616–623.

Uesugi, S. L., R. R. Yarwood, J. S. Selker, and P. J. Bottomley (2001), A model that uses the induction phase of lux gene-dependent bioluminescence in *Pseudomonas fluorescens* HK44 to quantify cell density in translucent porous media, *J. Microbiol. Methods*, 47, 315–322.

Wan, J. M., and T. K. Tokunaga (1997), Film straining of colloids in unsaturated porous media: Conceptual model and experimental testing, *Environ. Sci. Technol.*, 31, 2413–2420.

Wan, J. M., and T. K. Tokunaga (2005), Comments on "Pore-scale visualization of colloid transport and retention in partly saturated porous media," *Vadose Zone J.*, 4, 954–956.

Wan, J., and J. L. Wilson (1994), Visualization of the role of the gas-water interface on the fate and transport of colloids in porous media, *Water Resour. Res.*, 30, 11–23.

Wan, J. M., T. K. Tokunaga, C. F. Tsang, and G. S. Bodvarsson (1996), Improved glass micromodel methods for studies of flow and transport in fractured porous media, *Water Resour. Res.*, 32, 1955–1964.

Weisbrod, N., M. R. Niemet, and J. S. Selker (2002), Imbibition of saline solutions into dry and prewetted porous media, *Adv. Water Resour.*, 25, 841–855.

Weisbrod, N., M. R. Niemet, T. McGinnis, and J. S. Selker (2003a), Water vapor transport in the vicinity of imbibing saline plumes: Homogeneous and layered unsaturated porous media, *Water Resour. Res.*, 39(6), 1145, doi:10.1029/2002WR001539.

Weisbrod, N., M. R. Niemet, and J. S. Selker (2003b), Light transmission technique for the evaluation of colloidal transport and dynamics in porous media, *Environ. Sci. Technol.*, 37, 3694–3700.

White, D., M. M. Leifert, and K. K. Ryder (1996), Lux gene technology: A strategy to optimize biological control of soil-borne diseases, *New Phytol.*, 133, 173–181.

Wildenschild, D., J. Hopmans, C. Vaz, M. Rivers, D. Rikard, and B. Christensen (2002), Using X-ray computed tomography in hydrology: Systems, resolutions, and limitations, *J. Hydrol.*, 267, 285–297.

Yarwood, R. R., M. L. Rockhold, M. R. Niemet, J. S. Selker, and P. J. Bottomley (2002), Noninvasive quantitative measurement of bacterial growth in porous media under unsaturated-flow conditions, *Appl. Environ. Microbiol.*, 68, 3597–3605.

Yarwood, R., M. Rockhold, M. Niemet, J. Selker, and P. Bottomley (2006), Impact of microbial growth on water flow and solute transport in unsaturated porous media, *Water Resour. Res.*, 42, W10405, doi:10.1029/2005WR004550.

Yoon, J. S., J. T. Germaine, and P. J. Culligan (2006), Visualization of particle behavior within a porous medium: Mechanisms for particle filtration and retardation during downward transport, *Water Resour. Res.*, 42, W06417, doi:10.1029/2004WR003660.

Zevi, Y., A. Dathe, J. F. McCarthy, B. K. Richards, and T. S. Steenhuis (2005), Distribution of colloid particles onto interfaces in partially saturated sand, *Environ. Sci. Technol.*, 39, 7055–7064.

Zhang, P., and Y. Wang (2006), Epi-fluorescence imaging of colloid transport in porous media at decimeter scales, *Environ. Sci. Technol.*, 40(19), 6064–6069, doi:10.1021/es061104y.

————————————————

E. L. Kraft and J. S. Selker, Department of Biological and Ecological Engineering, Oregon State University, Gilmore Hall, Room 116, Corvallis, OR 97331-3609, USA. (krafte@engr.orst.edu)

N. Ochiai, Department of Crop and Soil Science, Oregon State University, Corvallis, OR 97331, USA.